Available online at www.sciencedirect.com
ScienceDirect
Journal of the European Ceramic Society 31 (2011) 773–782
www.elsevier.com/locate/jeurceramsoc

Synthesis, spark plasma sintering and electrical conduction mechanism in $BaTiO_3$–Cu composites

Songhak Yoon [a,*], Jürgen Dornseiffer [b], Yan Xiong [c], Daniel Grüner [c], Zhijian Shen [c], Shoichi Iwaya [d,e], Christian Pithan [a], Rainer Waser [a]

[a] *Institute for Solid State Research, Forschungszentrum Jülich GmbH, D-52425 Jülich, Germany*
[b] *Institute for Chemistry and Dynamics of the Geosphere, Forschungszentrum Jülich GmbH, D-52425 Jülich, Germany*
[c] *Arrhenius Laboratory, Stockholm University, SE-10691 Stockholm, Sweden*
[d] *IOM Technology Corporation, 957-0231 Shibata-shi, Japan*
[e] *Technical R&D Division, NAMICS Corporation, 108-0074 Tokyo, Japan*

Received 15 June 2010; received in revised form 29 October 2010; accepted 21 November 2010
Available online 14 December 2010

Abstract

$BaTiO_3$–Cu composite powders were prepared via an alkoxide-mediated synthesis approach. As-synthesized $BaTiO_3$ nanoparticles were as small as 40 nm and coated partially larger Cu particles of approximately 1 μm in size. Thermogravimetric analysis (TGA) and dilatometry revealed a gradual increase in weight loss and retarded shrinkage with the increase of Cu addition. $BaTiO_3$–Cu composites were successfully densified by spark plasma sintering (SPS). The microstructures show an average grain-size for $BaTiO_3$ of around 100 nm and a crystallite size of about 1 μm for the Cu inclusions. The AC conductivity of the $BaTiO_3$–Cu composites increased with increasing Cu content or with temperature. The dominant electrical conduction mechanism in SPSed $BaTiO_3$–Cu composites changed from migration of oxygen vacancies to band conduction of trapped electrons in oxygen vacancies with the increase of Cu content.

Keywords: Spark plasma sintering; Composites; Electrical conductivity; Densification

1. Introduction

Over the past few decades considerable efforts have been undertaken regarding the synthesis and fabrication of different nanocomposites. Ceramic–metal nanocomposites represent one of the promising candidate materials for multifunctional devices due to their exceptional mechanical, optical or electrical properties.[1–3] Of particular interest for energy-storage devices are nanocomposites composed of $BaTiO_3$ and metals (or polymers).[4–6] $BaTiO_3$ is one of the most studied ferroelectric materials and has been an important electronic material, as it is widely used as thermistors, capacitors, gate dielectrics, memories, and power-storage devices due to its high dielectric constant.[7–9]

The dielectric behavior of ceramic–metal composites has attracted much attention for many years due to the enhanced permittivity in the vicinity of the percolation threshold.[10–15] According to percolation theory, exceptional high values of permittivity can be achieved when the volume fraction of the conductive metallic phase approaches a certain critical value, the so-called percolation threshold where both the conductivity as well as the permittivity of the composite usually increase by several orders of magnitude.[16–18] It is anticipated, although not proven, that a large effect of permittivity enhancement can be achieved for a very intimate mixture of the metallic and dielectric phase. Even though many researchers have evidenced the colossal or giant permittivity of ceramic–metal composites, there are only some reports on the detailed analysis of electrical conductivity in such materials.

Since Flaschen first proposed the synthesis of crystalline barium titanate by an alkoxide-hydroxide route, quite a number of reports have been devoted to this process with small modifications of the synthetic procedure.[19–24] The main merit of the alkoxide-hydroxide route is the rather simple approach to form

* Corresponding author. Tel.: +49 (0)2461 61 5016; fax: +49 (0)2461 61 2550.
E-mail addresses: s.yoon@fz-juelich.de, songhak.yoon@empa.ch (S. Yoon).

0955-2219/$ – see front matter © 2010 Elsevier Ltd. All rights reserved.
doi:10.1016/j.jeurceramsoc.2010.11.012

crystalline $BaTiO_3$ nanoparticles at low temperatures well below 100 °C without the need of any further calcination treatments. It is believed that a rationally modified synthetic route can also be adapted for the preparation of $BaTiO_3$–Cu composite powders. Not only the development of a new synthetic route, but also an advanced sintering method had to be adopted in order to obtain a microstructure with metallic inclusions of Cu homogeneously dispersed in an ultrafine ceramic matrix of $BaTiO_3$. Much effort concerning the control of the size and distribution of metal nanoparticles has been undertaken in this context but only microcomposites have been reported so far. As mentioned above, it is believed that the realization of uniformly distributed metal particles within a ceramic matrix is a prerequisite for achieving good percolative ceramic–metal nanocomposites as a rather novel concept of dielectric materials. In this study, spark plasma sintering (SPS) has been carried out to successfully consolidate $BaTiO_3$–Cu powders into composites preserving ultrafine microstructures. Because SPS offers the combined advantages of fast heating rates, the application of mechanical pressure, very short sintering times and relatively low sintering temperatures, this technique provides an effective approach to promote densification and to reduce grain coarsening during sintering of nano- or submicron-composite powders.[25,26] To the best of our knowledge, the synthesis and spark plasma sintering of $BaTiO_3$–Cu composite powders have not been reported to date. In the present study, such powders were synthesized via an alkoxide-mediated method and consolidated by SPS. The characteristics of the as-synthesized powders, their sintering behavior, microstructure evolution as well as the resulting electrical properties have been investigated and are reported here.

2. Experimental procedures

2.1. Synthesis of $BaTiO_3$–Cu composite powders

$BaTiO_3$–Cu composite powders were prepared through an alkoxide-hydroxide sol-precipitation technique. During the hydrolysis and condensation of barium hydroxide octahydrate ($Ba(OH)_2{\cdot}8H_2O$; purity > 98%, Alfa Aesar GmbH & Co. KG, Karlsruhe, Germany) and titanium (IV) isopropoxide ($Ti[OCH(CH_3)_2]_4$; purity > 97%, Alfa Aesar GmbH & Co. KG) an alcoholic dilution of a commercial Cu paste (XK6078U, NAMICS Corporation, Niigata, Japan) was introduced. For this purpose different amounts of Cu paste were dissolved in 6 mol of isopropanol (C_3H_7OH, 99.8%, Merck KGaA, Darmstadt, Germany) at room temperature, respectively. Ultrasonic homogenization (SONOPULS, BANDELIN Electronic GmbH & Co. KG, Berlin, Germany) was applied for 10 min in order to well disperse the metal particles. Titanium (IV) isopropoxide (0.03 mol) was added into this solution followed by sonification for 10 min. Barium hydroxide octahydrate (0.03 mol) was added to deionized degassed water (18 mol) at room temperature while stirring vigorously. Then this aqueous solution of barium hydroxide octahydrate was heated to 80 °C at a rate of 2 °C/min. As soon as the solution temperature reached at 80 °C the as-prepared isopropanolic solution of Cu paste and titanium (IV) isopropoxide was added slowly. Seven different

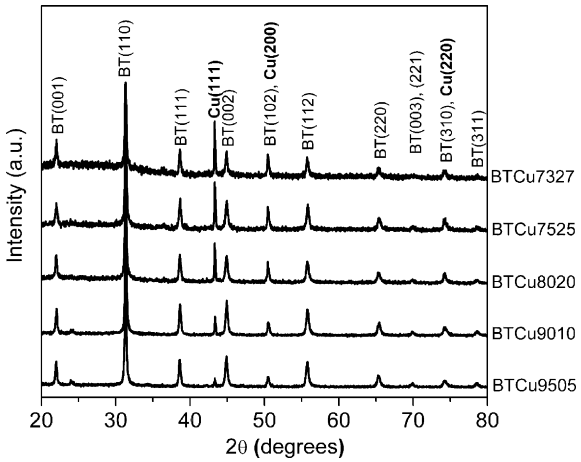

Fig. 1. X-ray diffraction patterns of the synthesized $BaTiO_3$–Cu composite powders (BT: $BaTiO_3$).

$BaTiO_3$–Cu composite powders with different volume fractions of Cu were prepared: 5, 10, 15, 20, 23, 25, and 27 vol.%. They are denoted as BTCu9505, BTCu9010, BTCu8515, BTCu8020, BTCu7723, BTCu7525, and BTCu7327, respectively in the following. After 15 min of refluxing at 80 °C the solutions were decanted and the isolated precipitates were dried at 80 °C for 12 h in a drying oven.

2.2. Spark plasma sintering of $BaTiO_3$–Cu composite powders

In order to densify the $BaTiO_3$–Cu composite powders spark plasma sintering (SPS) has been carried out using a Dr. Sinter 2050 apparatus (SPS Syntex Inc., Sumitomo Coal Mining Co., Tokyo, Japan). SPS allows densification at relatively low temperatures compared to conventional sintering. Through the application of mechanical pressure and an electrical discharge coarsening due to extensive grain-growth can substantially be limited. In a typical processing cycle powder (1.6–2.6 g) was loaded into a graphite pressure die (inner diameter of 12 mm). This powder containing die was then heated under vacuum first up to 600 °C by a preset program within 3 min and above this temperature a heating rate of 100 °C/min was applied until the final sintering temperature (T_F = 950 °C) was reached. The temperature was measured with an optical pyrometer focused on the surface of the graphite die and automatically regulated from 600 °C to the final sintering temperature. An uniaxial pressure of 75 MPa was applied after reaching T_F and a dwelling time of 5 min was kept for sintering. It is previously reported that the application of mechanical pressure at T_F generally results in a much finer microstructure than if the pressure is already applied before or during heating up.[27]

2.3. Characterization of the synthesized composite powders and the resulting sintered bodies

With the synthesized composite powders, phase identification was performed by powder X-ray diffraction (XRD, Philips X'PERT, Koninklijke Philips Electronics N.V., Amsterdam,

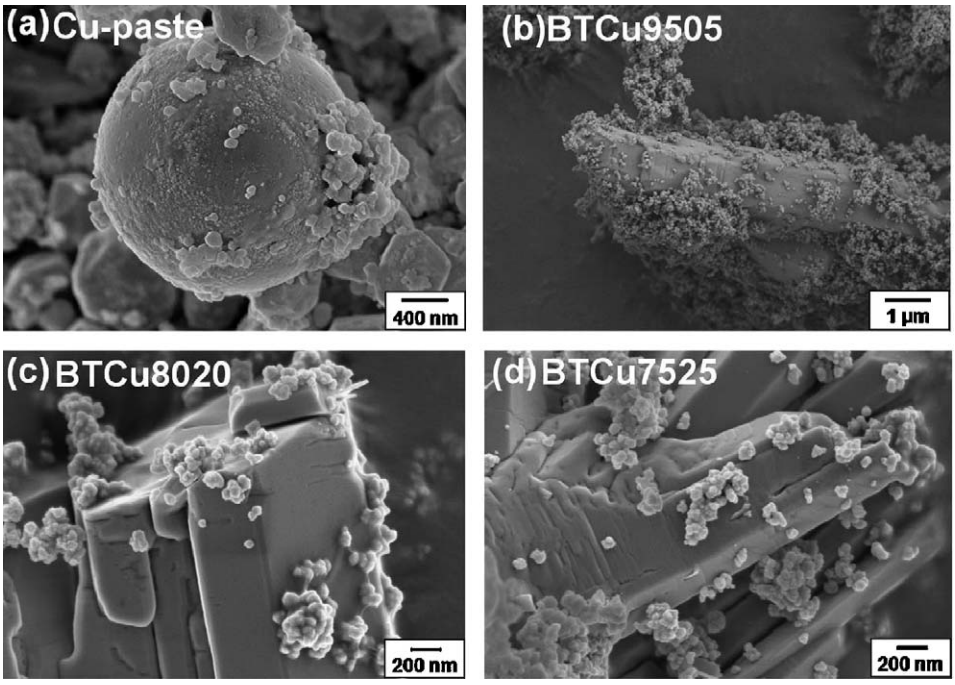

Fig. 2. Scanning electron microscopy (SEM) micrographs of $BaTiO_3$–Cu composite powders.

the Netherlands) using Cu-Kα radiation with a wavelength of λ = 1.5418 Å. The respective diffraction patterns were recorded from 20° to 80° (2θ) with an angular step interval of 0.02°.

Densities were measured with an accuracy of 0.001 g/cm^3 by immersing the compacts into water and determining their volume using the Archimedes principle. The particle size, their distribution and their morphology in the synthesized composite powders were studied by field emission scanning electron microscopy (FE-SEM, LEO1530, Carl Zeiss AG, Jena, Germany) operating at 20 kV and transmission electron microscopy (TEM, CM-200, Koninklijke Philips Electronics N.V., Amsterdam, the Netherlands) operating at 200 kV. Electron microscopy (FE-SEM and TEM) was also used for microstructural characterization of the consolidated composite compacts. The study of the heterogeneous microstructures of the sintered bodies consisting of rather small and soft inclusions of metallic Cu in an ultrafine matrix of ceramic $BaTiO_3$ is inherently difficult because the preparation of microsections by conventional mechanical polishing often easily introduces artifacts. These difficulties were circumvented by using an argon ion milling system to polish the composite surfaces with little mechanical impact only. Analytical TEM investigations were carried out on sintered composites in order to gain element mappings by energy dispersive X-ray spectroscopy (EDS). The focused ion beam (FIB) technique was applied to prepare the analytical TEM samples. For this purpose, the composite samples were thinned down to 100 nm thickness with a gallium ion beam. The size distribution of Cu inclusions was determined from images obtained with an optical microscope (Axioplan 2, Carl Zeiss AG, Jena, Germany) equipped with a digital microscope camera (ProgRes CF, Jenoptik GmbH, Jena, Germany) and an image acquisition software (ProgRes CapturePro).

Thermo-gravimetric analysis (TGA, STA 429, Netzsch Gerätebau GmbH, Selb, Germany) experiments were carried out under Ar atmosphere (10 ppm O_2) in a temperature range from 25 °C to 1050 °C with a heating and cooling rate of 20 °C/min in order to determine decomposition reactions and the herewith associated mass losses during further ceramic processing. Dilatometry (DIL 402C, Netzsch Gerätebau GmbH) was used to investigate the shrinkage behavior of the composite powders under Ar atmosphere (10 ppm O_2) in the temperature range from 25 °C to 1050 °C as well. The heating and cooling rate of the dilatometer was 20 °C/min. For this purpose cylindrical pellets with a diameter 10 mm were compacted by cold uniaxial pressing with a pressure of 63.7 MPa followed by cold isostatic compaction at 815 MPa (Weber Pressen KIP 40ES, Paul-Otto Weber GmbH, Remshalden, Germany). The green densities of all the powder pellets were in the range of 54.9–55.4% of the theoretical density independent of the Cu content.

For dielectric measurements, the top and bottom surface layers of sintered pellets were removed with SiC paper and subsequently polished with diamond paste down to 0.25 μm. After cleaning with isopropyl alcohol, electrodes of an InGa alloy with a molar ratio of 7:3 were painted onto the pellets. Conductivity measurements were performed in the frequency range from 1 Hz to 1 MHz with an applied AC voltage of 1.5 V for temperatures between 25 °C and 250 °C using an impedance analyzer (Alpha Dielectric Analyzer, NOVOCONTROL GmbH, Hundsangen, Germany). The measurement system consisted of a frequency response analyzer (Solartron SI 1260, Farnborough, U.K.) and a broadband dielectric converter (Novocontrol BDC, NOVOCONTROL GmbH). All electric measurements were carried out upon heating. The real part of complex conductivity σ' was calculated using the relation $\sigma' = \omega\varepsilon_0\varepsilon''$, with ω being the

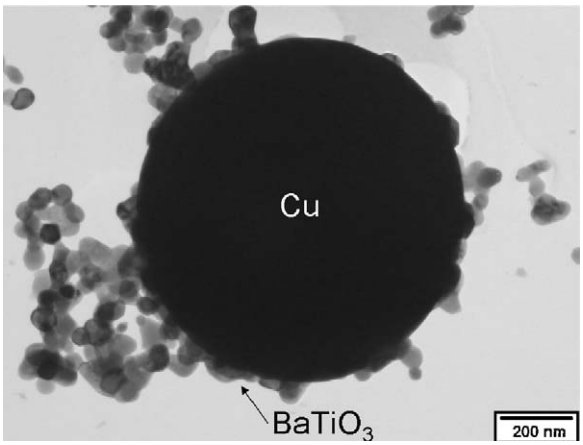

Fig. 3. Representative transmission electron microscopy (TEM) micrograph of $BaTiO_3$–Cu composite (BTCu8020) powders.

angular frequency, ε_0 the permittivity of vacuum and ε'', the imaginary part of permittivity of the measured material.

3. Results and discussion

Fig. 1 shows the X-ray diffraction patterns of the synthesized $BaTiO_3$–Cu composite powders. All peaks were identified to originate either from pure $BaTiO_3$ (JCPDS 31-0174) or from Cu (JCPDS 04-0836) and no secondary phases could be found, suggesting that no detectable reaction took place between $BaTiO_3$ and Cu during the synthesis. As expected the relative diffraction intensities of the Cu reflections compared to the ones of $BaTiO_3$ increased with the increase of Cu content. The evolution of the XRD-peaks confirms the successful composition control during synthesis.

The phase morphology of the as-synthesized $BaTiO_3$–Cu composite powders is shown in Fig. 2. The average Cu particle size was about 1 μm (Fig. 2(a)) but rather large rod-shaped particles of several tens of microns in length can be frequently found as well (Fig. 2(b)–(d)). The average particle size of $BaTiO_3$ was about 40 nm. Cu particles covered by aggregated $BaTiO_3$ nanoparticles can be recognized in some areas. A representative bright-field TEM image of the as-synthesized $BaTiO_3$–Cu composite powders is shown in Fig. 3. This TEM-observation under high magnifications clearly reveals that thin layers of $BaTiO_3$ are formed on the surface of the Cu particles, evidencing the successful coating of metallic particles by the dielectric phase.

Fig. 4 shows results from the thermogravimetric analysis (TGA) of $BaTiO_3$–Cu composite powders. The TGA traces show several successive steps of mass losses. The first one occurs between room-temperature up to approximately 500 °C and is attributed to the release of organics stemming from the Cu-phase and physisorbed water on the surface of the $BaTiO_3$ nanopowders.[28,29] The second weight loss is observed for a wide range of temperatures up to 1000 °C and is also strongly dependent on the Cu content. It mainly results from the release of chemisorbed water and/or incorporated hydroxyl ions in the lattice of $BaTiO_3$. The weight losses as a function of Cu content at 500 °C and 1000 °C increase with growing Cu content (inset in Fig. 4). It is apparent that with the increase of Cu addition, $BaTiO_3$–Cu nanopowders show increased weight losses due to higher concentrations of organics, water, and hydroxyl ions.

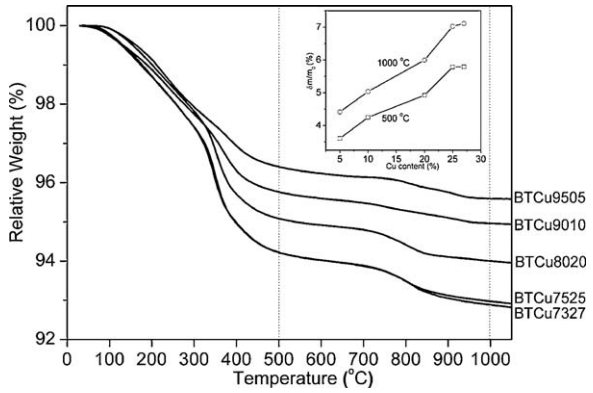

Fig. 4. TGA of $BaTiO_3$–Cu composite powders (Ar atmosphere with 10 ppm O_2). Percentage of weight loss in dependence of Cu content at 500 °C and 1000 °C is plotted in an inset.

Dilatometric measurements were carried out in order to study the sinterability of the synthesized composite nanopowders. The linear shrinkage curves of the samples are presented in Fig. 5. The degree of linear shrinkage was almost independent from the Cu content up to 15 vol.% of Cu addition and the shrinkage rate $(\delta L/L_0)/\delta T$ seems to be slightly higher for the compositions with 15 vol.% of Cu. Between 15 and 27 vol.% of Cu addition, the maximum shrinkage decreases with increasing Cu content. The difference of the agglomeration degree in every composite composition can be one reason of different shrinkage behavior but further studies are needed to clarify the exact shrinkage behavior of $BaTiO_3$–Cu composites.

Fig. 6 represents one example of the linear shrinkage during spark plasma sintering for our $BaTiO_3$–Cu composites. All samples show a drastic increase of the shrinkage rate around the final sintering temperature ($T_F = 950$ °C), where uniaxial pressure was applied. A gradual increase of shrinkage is observed with increasing Cu content even before pressure was applied,

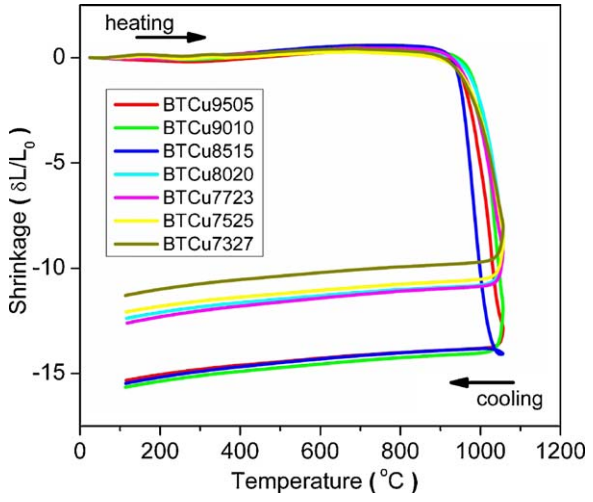

Fig. 5. Dilatometric shrinkage curves of $BaTiO_3$–Cu composite powders (Ar atmosphere with 10 ppm O_2).

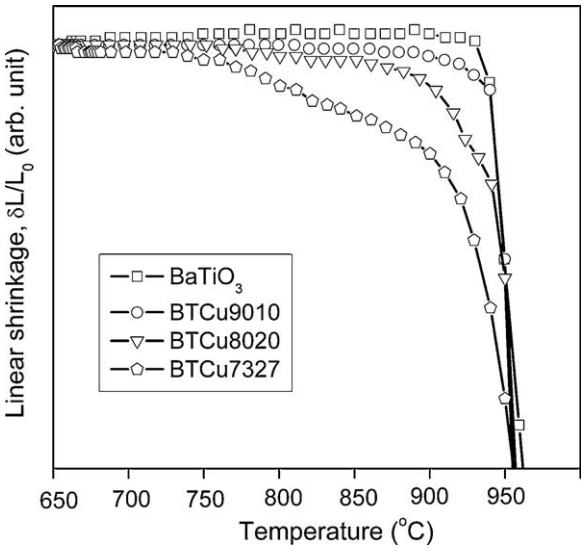

Fig. 6. Linear shrinkage during spark plasma sintering for $BaTiO_3$–Cu composite powders for selected compositions at a maximum sintering temperature $T_F = 950\,^{\circ}C$.

which confirms that pre-sintering of $BaTiO_3$–Cu composite is enhanced through the addition of Cu.

The dependence of the relative density of $BaTiO_3$–Cu composites from the metal content after the spark plasma sintering (SPS) is shown in Fig. 7. The relative densities of the compacts were larger than 86.3% for all compositions, a value that could not be reached by conventional sintering at 950 °C. The relative density of the composites increased to a maximum value of 93.9% up to 20 vol.% of Cu addition. With the introduction of metal particles into a matrix of $BaTiO_3$, the ductile metal particles apparently enhance the sinterability of the composite compared to pure $BaTiO_3$. Above 20 vol.% of Cu addition, however, a gradual decrease of the final density was observed. From the standpoint of optimum density after sintering at $T_F = 950\,^{\circ}C$, the Cu content of 20 vol.% can be regarded as a critical value, which is consistent with our dilatometric measurements.

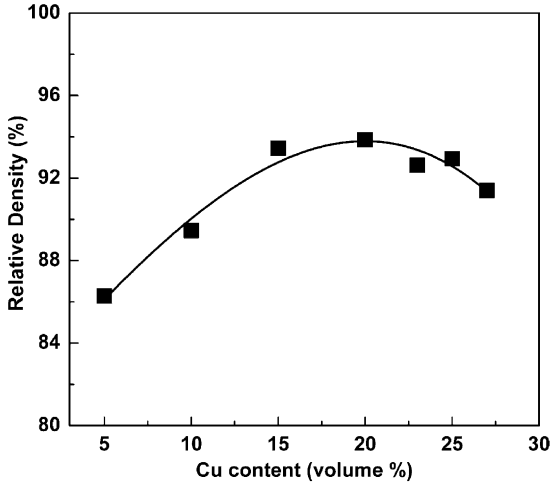

Fig. 7. Relative density as a function of the volume fraction of Cu.

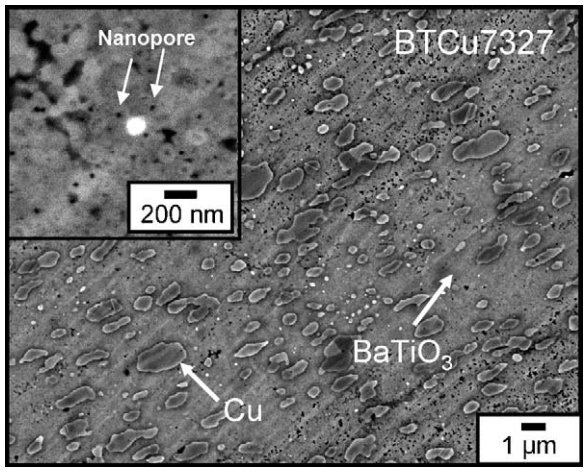

Fig. 8. Scanning electron microscopy (SEM) micrographs of $BaTiO_3$–Cu composite BTCu7327 after sintering at 950 °C. Nanograins of the $BaTiO_3$-matrix and nanopores are shown in the inset.

The microstructure of BTCu7327 after SPS at 950 °C is shown in Fig. 8. The nanocrystalline character of the $BaTiO_3$-matrix was retained with an average grain-size around 100 nm as shown in the inset. In certain areas, however, grains of about 1 μm in size were also observed. The size of the Cu inclusions as they are visible in the micrographs varies from 100 nm to a few microns. Nanosized pores also can be found in the area where fine $BaTiO_3$ nanograins are present, indicating that retarded grain growth in $BaTiO_3$ is related with poor densification. In the area of grown $BaTiO_3$ grains with an average grain size of about 1 μm, however, such pores can be hardly found implying that grains grow to a larger extent in these regions and that densification is almost completed here. Up to 27 vol.% of Cu addition, any possibility of percolation was not found.

Fig. 9 shows the size distribution of the Cu inclusions in BTCu7327 by volumetric and numeral percentages. Individual Cu inclusions were assumed as spheres and particles smaller

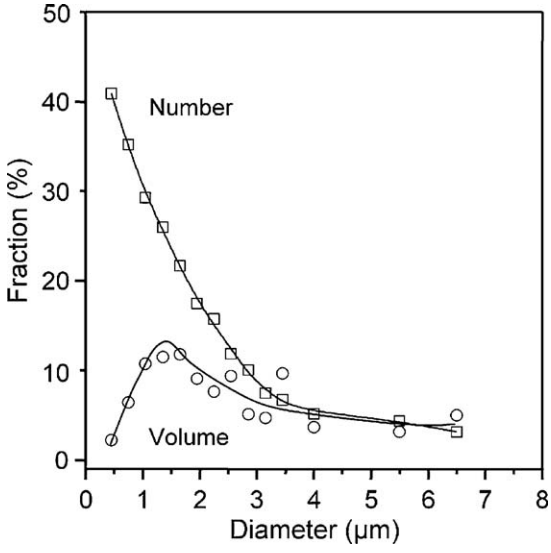

Fig. 9. Volume and number fraction of Cu inclusion as a function of their size in diameter for $BaTiO_3$–Cu composite BTCu7327.

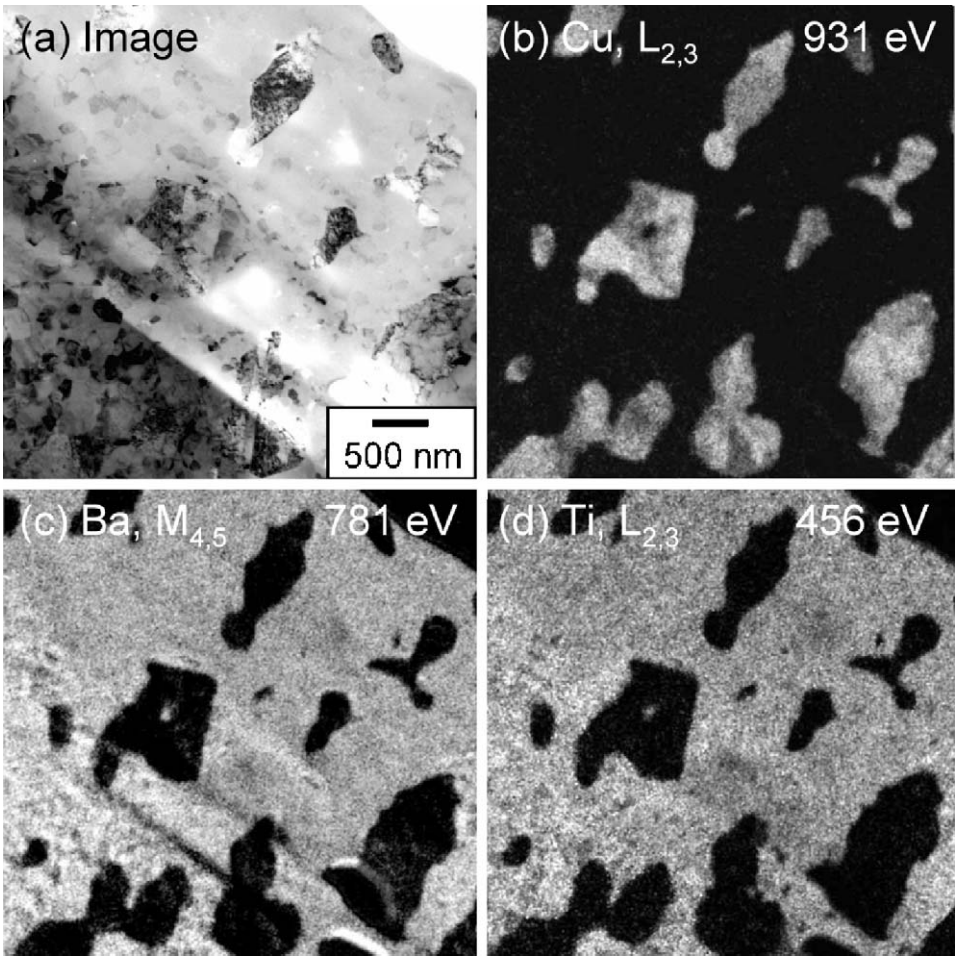

Fig. 10. Element distribution of $BaTiO_3$–Cu composite BTCu7327 recorded by energy dispersive X-ray spectroscopy. Characteristic X-ray intensities of each element are measured and recorded as image brightness, which is proportional to the local relative concentration of the elements in TEM.

than 300 nm could not be evaluated due to the resolution limit of the instrument. Here it should be noted that the volume fraction of ultrafine Cu inclusions less than 1 μm is relatively large (12%) which is much more than that would be expected from a purely statistical distribution resulting from cutting equiaxed Cu particles of 1 μm (initial Cu particle size from paste). The mean value of the inclusion size was 830 nm regarding their number and 1.18 μm with respect to their volume fraction. For this reason the assumption that the rather large original micron-sized Cu particles of the paste are also dismantled during SPS into smaller ones to some extent seems to be feasible.

Element mapping was carried out using TEM in order to study the distribution of $BaTiO_3$ and Cu grains in the sintered composites in more detail (Fig. 10). Individual Cu crystals of about 500 nm or less in diameter can be recognized by the uniform distribution of the element Cu as bright area shown in Fig. 10(b). This result also clearly supports the assumption that Cu particles may have melted locally (melting point of bulk Cu: 1084 °C) and are dismantled down to 500 nm or less due to the intensive Joule heating from the pulsed electric current and spark discharges between the particles during SPS.[30] Also the rather irregular shape of the Cu-phase indicates that probably through the simultaneous action of temperature, mechanical pressure and electric discharge during SPS, local melting or at least softening of Cu and subsequent plastic flow into open pores might have taken place. The elements Ba and Ti are concentrated on other regions of the investigated area (Fig. 10(c) and (d)).

Fig. 11 represents the variation of the real part of AC conductivity (σ') as a function of frequency for different Cu additions at room temperature. The AC conductivity gradually increases with increasing Cu content. At low frequencies a plateau which is more pronounced for larger Cu contents than for smaller ones reflects the DC conductivity (σ_{dc}) of the samples and at high frequencies a dispersive region, the so-called "universal dielectric response" (UDR) appears. It can approximately be described by a power law.[31] The threshold value at which the conductivity plateau at low frequencies begins to disperse shifts to higher frequencies with increasing Cu content.

Fig. 12 shows the frequency dependence of σ' for BTCu8020 for some selected temperatures. It is clear that the AC conductivity increases with increasing measuring temperature. The threshold frequency of dispersion shifts again to higher frequency with increasing temperature. A pronounced plateau in the frequency region measured here appeared above 120 °C. The σ_{dc} values corresponding to this plateau for the low frequency region follow an Arrhenius type relationship as shown

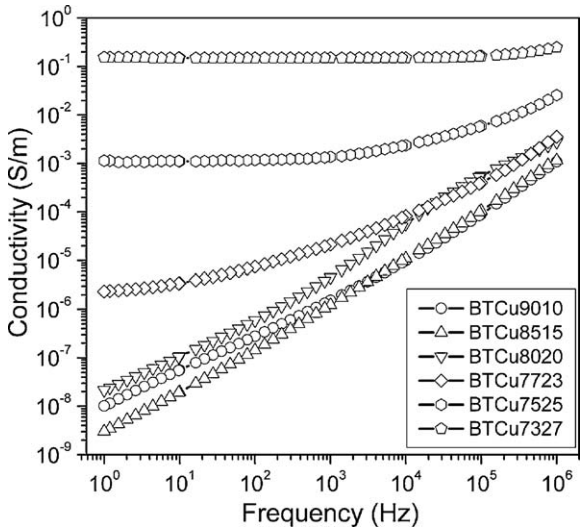

Fig. 11. Frequency dependence of the real part of AC conductivity at room temperature for different Cu contents in $BaTiO_3$–Cu composites.

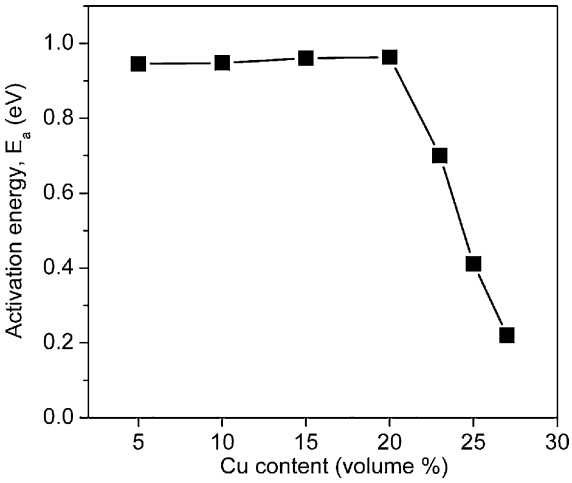

Fig. 13. Activation energy as a function of Cu content.

in Fig. 12(b),

$$\sigma_{dc} = \sigma_0 \exp\left(-\frac{E_a}{k_B \cdot T}\right) \quad (1)$$

where E_a is the activation energy of electrical conduction, k_B the Boltzmann's constant, T the absolute temperature and σ_0 is a pre-exponential factor. The solid line is the best-fit curve of the equation and the activation energy (E_a) for conduction was determined to be 0.969 eV.

Fig. 13 represents the dependence of the thermal activation energy E_a on the Cu content. Below a critical value x_c of 20 vol.% E_a remains almost constant at a level of around 0.954 eV and above x_c E_a shows a linear decrease down to 0.220 eV for 27 vol.% of Cu addition. The activation energies in all samples are much smaller than the band gap for intrinsic electronic conduction in $BaTiO_3$ (approximately 3 eV),[32,33] indicating that extrinsic conduction mechanisms associated with defects are dominant in all samples.

A number of previous reports have shown that an activation energy of about 0.9 eV is required for oxygen vacancy diffusion.[34–37] Activation energy for electromigration of oxygen vacancies was found to be about 0.9 eV, for instance in the study on resistance degradation of perovskite-type titanates.[34] West et al. reported that the activation energy for the creation of oxygen vacancies assisting the migration of oxygen ions was about 0.92 eV,[37] which fits to the data presented here. On the other hand, for a single-domain crystal of *n*-type $BaTiO_3$, Berglund and Braun have shown that impurity states approximately 0.2–0.3 eV below the conduction band are associated with oxygen vacancies and band conduction.[38] This activation energy (donor level) is required to activate an trapped electron from oxygen vacancies to a higher energy level in the conduction band. For our sintered $BaTiO_3$–Cu composites, the activation energy for electrical conduction is likely to consist of a combination of the migration energy for oxygen vacancies dominating below x_c and the energy for band conduction of electrons trapped by oxygen vacancies above x_c. In other words, there is probably a crossover of two conduction mechanism regimes for $BaTiO_3$–Cu composites. This change of electrical conduction from migration of oxygen vacancies to the motion of delocalized electrons trapped in oxygen vacancies is manifested by a sudden decrease of the activation energy above a metal content of 20 vol.%. Gilbert et al. have reported for $BaTiO_3$ thin films that the thermal activation energy for electrical conduction depends

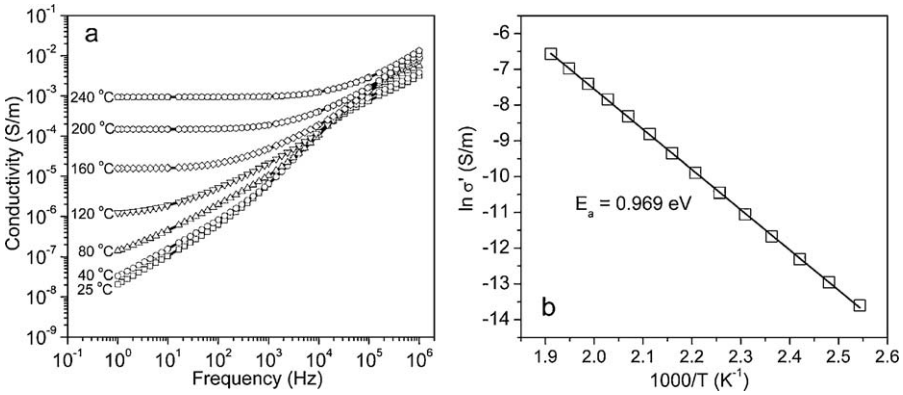

Fig. 12. (a) Frequency dependence of the AC conductivity of the $BaTiO_3$–Cu composite BTCu8020 for selected temperatures in log–log plot and (b) Arrhenius plots of the temperature dependence of DC conductivity for the $BaTiO_3$–Cu composite BTCu8020.

on the resistivity of the samples. They identified three different regimes.[39] In the case of high resistivity ρ ($\rho > 10^4\ \Omega\,m$) E_a is in the order of 0.36–0.50 eV. For intermediate resistivities ($10^1\ \Omega\,m < \rho < 10^4\ \Omega\,m$) E_a is almost constant at 0.20 eV and a continuous decrease was observed for resistivities below 10 Ω m due to an increasing number of additional charge carriers. For our sintered $BaTiO_3$–Cu composites, however, E_a is fairly constant at 0.954 eV in a region where resistivity was higher than $10^6\ \Omega\,m$ and a continuous decrease down to 0.220 eV was observed for resistivities less than $10^6\ \Omega\,m$. This discrepancy may originate from a difference in the concentration of oxygen vacancies. Further studies would be necessary to address this issue in more detail. Steinsvik et al. also showed that the activation energy for electric conduction in the ABO_3–type perovskite structure decreases with increasing oxygen vacancy content.[40]

The present $BaTiO_3$–Cu composites were sintered under vacuum the level of which typically was 1–10 Pa (oxygen partial pressure $p(O_2) \approx 2.06 \times 10^{-6}$ to 2.06×10^{-5} atm) during SPS. However, all composite powders were surrounded by a graphite sheet and die during processing, which provide a strongly reducing atmosphere during SPS. For the oxidation of carbon to carbon monoxide at 950 °C according to

$$\frac{1}{2}O_2 + C \leftrightarrow CO \tag{2}$$

the equilibrium value of $p(O_2)$ amounts to 5.72×10^{-18} atm. On the other hand the equilibrium oxygen partial pressure for oxygen for the oxidation of carbon monoxide to carbon dioxide

$$\frac{1}{2}O_2 + CO \leftrightarrow CO_2 \tag{3}$$

at a sintering temperature of 950 °C is about 2.61×10^{-14} atm. In the case of oxidation of copper to copper (II) oxide at this temperature

$$\frac{1}{2}O_2 + Cu \leftrightarrow CuO \tag{4}$$

the equilibrium partial pressure is about 1.12×10^{-7} atm. The copper metal particles in our composite powders are not oxidized during SPS as confirmed by XRD (not shown here). According to the defect model proposed by Chan et al.,[41,42] the reduction reaction in the region of low $p(O_2)$ is

$$O_o \leftrightarrow \frac{1}{2}O_2 + V_o^{\bullet\bullet} + 2e^- \tag{5}$$

At 950 °C and very low oxygen partial pressures below 10^{-14} atm the formation of oxygen vacancies and electrons dominates the defect chemistry of nominally undoped $BaTiO_3$. Thus, it is believed that rather large numbers of oxygen vacancies can be produced, releasing electrons to the conduction band. In the intermediate oxygen partial pressure regime between 10^{-14} atm and 10^{-4} atm, frozen acceptor states trap electrons created through the formation of oxygen vacancies and in this region the concentration of oxygen vacancies remains constant at 950 °C. The intrinsic minimum of conductivity determined by the ionization across the band gap

$$\text{Nil} \leftrightarrow e^- + h^+ \tag{6}$$

occurs at $p(O_2) \approx 10^{-4}$ atm. Above this partial pressure oxygen vacancies are further gradually filled and the formation of holes in the valence band results in a *p*-type conduction behavior. For our $BaTiO_3$–Cu composites, due to the reducing effect of graphite during SPS, the reduction reaction in the region of low $p(O_2)$ can be described by Eq. (2).

Up to the critical Cu content x_c conductivity remains low at 1 Hz and the activation energy is constant. Probably conductivity is determined by oxygen vacancies. The concentration of oxygen vacancies remains possibly almost constant until x_c and electrons created by the formation of oxygen vacancies are trapped by naturally occurring acceptors. At higher Cu additions conductivity increases by 7 orders of magnitude and the global activation energy gradually decreases from approximately 0.954 eV down to 0.220 eV at 27 vol.% of Cu addition. Apparently large numbers of additional charge carriers are being generated in the bulk and the formation of these charge carriers by thermal activation becomes easier. As additional donors below the conduction band – for instance singly ionized oxygen vacancies – can be created (donor level of singly ionized oxygen vacancies is located approximately 0.2 eV below the conduction band). Here the question arises where these additional donors come from. A possible explanation for our observation can be given by the role of the Cu phase acting as a getter to oxygen from $BaTiO_3$. Thus copper is probably only slightly oxidized on the interface to the ceramic phase. With the increase of Cu content, gradually additional oxygen uptake from the $BaTiO_3$ lattice could take place. In other words, below x_c, the electrical conduction is mainly dominated by the migration of oxygen vacancies since the concentration of electrons is not high enough to dominate the electrical conduction. Above x_c, however, a larger amount of oxygen vacancies is generated, providing trapping sites for electrons and thermally enhanced conduction presumably occurs by excitation of trapped electron in oxygen vacancies.

Although the solubility of $BaTiO_3$ for Cu is extremely small, one might also speculate that the amount of acceptor centers (Cu''_{Ti}) would increase with increasing Cu addition through the incorporation of Cu^{2+} into the $BaTiO_3$ lattice. This "acceptor" effect, however, requires interdiffusion and the motion of Ti-vacancies. At 950 °C, diffusion of Ti-vacancies, however, is extremely slow. The calculated mean diffusion path of Ti vacancies is about 10 nm for the present sintering conditions (5 min, 950 °C). Therefore, this effect can be neglected for kinetic reason. Moreover, the conductivity of $BaTiO_3$–Cu composites increases with increasing Cu content. If Cu could be incorporated into the $BaTiO_3$ lattice as an acceptor, the concentration of conduction electrons should be decreased due to additional electron trapping by the incorporation of the acceptor ions. This is the opposite of our observation. Instead of trapping in singly ionized oxygen vacancies, electrons might also be captured by Ti^{4+} in $BaTiO_3$ resulting in Ti^{3+}. The presence of a large amount of Ti^{3+} ions on Ti^{4+} sites would then

lead to the hopping of small polarons. However, the activation energy for hopping of small polarons between Ti^{4+} and Ti^{3+} ions in reduced $BaTiO_3$ was reported to be situated in the range 0.068–0.074 eV,[43–45] values that are much smaller than the ones observed in $BaTiO_3$–Cu composites. Small polaron hopping might be a possible conduction mechanism for similar $BaTiO_3$–Ni composites.[46] The apparent difference of electrical conduction in $BaTiO_3$–Cu and –Ni composites could possibly originate from the concentration differences in oxygen vacancies and electrons formed through the different sintering conditions. Further investigations are needed to obtain a clear picture. In this context more detailed impedance analysis should also elucidate the various contributions of the microstructure such as $BaTiO_3$ grains, grain boundaries, and the $BaTiO_3$–Cu interfaces to capacitance (permittivity) and resistance (conductivity). It will be reported with a separate paper in which data analysis of impedance spectra would be discussed.

4. Summary

$BaTiO_3$–Cu composite powders consisting of mostly spherical shaped micron sized Cu-particles coated by $BaTiO_3$ nanocrystals were prepared via an alkoxide-mediated synthesis method. $BaTiO_3$ was found as aggregates built up of nanosized primary particles as small as 40 nm. With the introduction of Cu, TGA and dilatometric measurement show increased weight losses and retarded shrinkage at higher Cu contents. The composite powders were well densified by spark plasma sintering. AC conductivity of the resulting composites gradually increased with increasing Cu content and temperature. The dominant electrical conduction mechanism changes from migration of oxygen vacancies to band conduction of trapped electrons in oxygen vacancies.

Acknowledgements

This work was supported by the Korea Research Foundation Grant funded by the Korean Government (KRF-2007-D00124). S. Yoon acknowledges support from COST Action 539 (COST-STSM-539-03589) of the European Union. NAMICS Corporation, Niigata (Japan) is gratefully acknowledged for financial support within a common collaboration project. The authors are grateful to Dr. Heinz-Josef Penkalla for the element specific analysis by TEM and to Dr. Detlev Hennings for helpful discussion and comments.

References

1. Ajayan PM, Schadler LS, Braun PV. *Nanocomposite science and technology*. Weinheim, Germany: Wiley-VCH Verlag GmbH & Co; 2003.
2. Sekino T, Nakajima T, Ueda S, Niihara K. Reduction and sintering of a nickel-dispersed alumina composite and its properties. *J Am Ceram Soc* 1997;**80**:1139–48.
3. Cho WW, Kagomiya I, Kakimoto K-I, Ohsato H. Paraelectric ceramics/metal dual composites $SrTiO_3$/Pt system with giant relative permittivity. *Appl Phys Lett* 2006;**89**:152905.
4. Kim P, Jones SC, Hotchkiss PJ, Haddock JN, Kippelen B, Marder SR, et al. Phosphonic acid-modified barium titanate polymer nanocomposites with high permittivity and dielectric strength. *Adv Mater* 2007;**19**: 1001–5.
5. Yao S-H, Dang Z-M, Jiang M-J, Bai J. $BaTiO_3$–carbon nanotube/polyvinylidene fluoride three-phase composites with high dielectric constant and low dielectric loss. *Appl Phys Lett* 2008;**93**:182905.
6. Li J, Claude J, Norena-Franco LE, Seok SI, Wang Q. Electrical energy storage in ferroelectric polymer nanocomposites containing surface-functionalized $BaTiO_3$ nanoparticles. *Chem Mater* 2008;**20**: 6304–6.
7. Moulson AJ, Herbert JM. Temperature-sensitive resistors in electroceramics. *Materials, properties, applications*. 2nd ed. West Sussex, UK: John Wiley & Sons Ltd.; 2003. p. 159–73.
8. Phule PP, Risbud SH. Low-temperature synthesis and processing of electric materials in the BaO–TiO_2 system. *J Mater Sci* 1990;**25**:1169–83.
9. Hennings D, Klee M, Waser R. Advanced dielectrics: bulk ceramics and thin films. *Adv Mater* 1991;**3**:334–40.
10. Pecharromán C, Esteban-Betegón F, Bartolomé JF, López-Esteban S, Moya JS. New percolative $BaTiO_3$–Ni composites with a high and frequency-independent dielectric constant ($\varepsilon_r \approx 80\,000$). *Adv Mater* 2001;**13**: 1541–4.
11. Chen Z, Huang J, Chen Q, Song C, Han G, Weng W, et al. A percolative ferroelectric–metal composite with hybrid dielectric dependence. *Scr Mater* 2007;**57**:921–4.
12. Huang J, Cao Y, Hong M. Ag–$Ba_{0.75}Sr_{0.25}TiO_3$ composites with excellent dielectric properties. *Appl Phys Lett* 2008;**92**:022911.
13. Lin Y, Nan C-W, Wang J, Liu G, Wu J, Cai N. Dielectric behavior of $Na_{0.5}Bi_{0.5}TiO_3$-based composites incorporating silver particles. *J Am Ceram Soc* 2004;**87**:742–5.
14. López-Estebana S, Bartoloméa JF, Pecharromána C, Mello Castanhob SRH, Moya JS. Wet processing and characterization of ZrO_2/stainless steel composites: electrical and mechanical performance. *Mater Res* 2001;**4**:217–22.
15. Xiang P-H, Kinemuchi Y, Watari K. Enhanced dielectric properties of bismuth titanate/silver composites. *J Electroceram* 2006;**17**: 861–5.
16. Efros AL, Shklovskii BI. Critical behaviour of conductivity and dielectric constant near the metal–non-metal transition threshold. *Phys Status Solidi B* 1976;**76**:475–85.
17. McLachlan DS, Blaszkiewicz M, Newham RE. Electrical resistivity of composites. *J Am Ceram Soc* 1990;**73**:2187–203.
18. Brosseau C. Modelling and simulation of dielectric heterostructures: a physical survey from an historical perspective. *J Phys D: Appl Phys* 2006;**39**:1277–94.
19. Flaschen SS. An aqueous synthesis of barium titanate. *J Am Chem Soc* 1955;**77**:6194.
20. Kiss K, Meander J, Vukasovich MS, Lockhart RJ. Ferroelectric of ultrafine particle size: I, synthesis of titanate powders of ultrafine particle size. *J Am Ceram Soc* 1966;**49**:291–4.
21. Chaput F, Boilot J-P. Alkoxide-hydroxide route to synthesize $BaTiO_3$-based powders. *J Am Ceram Soc* 1990;**73**:942–8.
22. Golubko NV, Yanovskaya MI, Golubko LA, Kovsman EP, Listoshina MB, Rotenberg BA. Preparation of barium titanate and related materials by the alkoxide-hydroxide route. *J Sol–Gel Sci Technol* 2001;**20**: 135–43.
23. Kamiya H, Gomi K, Iida Y, Tanaka K, Yoshiyasu T, Kakiuchi T. Preparation of highly dispersed ultrafine barium titanate powder by using mircobial-derived surfactant. *J Am Ceram Soc* 2003;**86**:2011–8.
24. Qi JQ, Wang Y, Chen WP, Li LT, Chan HLW. Direct large-scale synthesis of perovskite barium strontium titanate nano-particles from solutions. *J Solid State Chem* 2005;**178**:279–84.
25. Viswanathan V, Laha T, Balani K, Agarwal A, Seal S. Challenges and advances in nanocomposite processing techniques. *Mater Sci Eng R* 2006;**54**:121–286.
26. Liu J, Shen Z, Nygren M, Su B, Button TW. Spark plasma sintering behavior of nano-sized (Ba, Sr)TiO_3 powders: determination of sintering parameters yielding nanostructured ceramics. *J Am Ceram Soc* 2006;**89**:2689–94.
27. Shen Z, Johnsson M, Zhao Z, Nygren M. Spark plasma sintering of alumina. *J Am Ceram Soc* 2002;**85**:1921–7.

28. Qi J, Li L, Wang Y, Gui Z. Preparation of nanoscaled $BaTiO_3$ powders by DSS method near room temperature under normal pressure. *J Cryst Growth* 2004;**260**:551–6.
29. Kumar V. Solution-precipitation of fine powders of barium titanate and strontium titanate. *J Am Ceram Soc* 1999;**82**:2580–4.
30. Song X, Liu X, Zhang J. Neck formation and self-adjusting mechanism of neck growth of conducting powders in spark plasma sintering. *J Am Ceram Soc* 2006;**89**:494–500.
31. Jonscher AK. The universal dielectric response. *Nature* 1977;**267**:673–9.
32. Hirose N, West AR. Impedance spectroscopy of undoped $BaTiO_3$ ceramics. *J Am Ceram Soc* 1996;**79**:1633–41.
33. Baer WS. Interband Faraday rotation in some perovskite oxides and rutile. *J Phys Chem Solids* 1967;**28**:677–87.
34. Waser RM. Electrochemical boundary-conditions for resistance degradation of doped alkaline-earth titanates. *J Am Ceram Soc* 1989;**72**:2234–40.
35. Lockämper R, Neumann H, Arlt G. Internal bias in acceptor-doped $BaTiO_3$ ceramics: numerical evaluation of increase and decrease. *J Appl Phys* 1990;**68**:4220–4.
36. Warren WL, Vanheusden K, Dimos D, Pike GE, Tuttle BA. Oxygen vacancy motion in perovskite oxides. *J Am Ceram Soc* 1996;**79**:536–8.
37. West AR, Adams TB, Morrison FD, Sinclair DC. Novel high capacitance materials: $BaTiO_3$:La and $CaCu_3Ti_4O_{12}$. *J Euro Ceram Soc* 2004;**24**:1439–48.
38. Berglund CN, Braun HJ. Optical absorption in single-domain ferroelectric barium titanate. *Phys Rev* 1976;**164**:790–9.
39. Gilbert SR, Wills LA, Wessels BW, Schindler JL, Thomas JA, Kannewurf CR. Electrical transport properties of epitaxial $BaTiO_3$ thin films. *J Appl Phys* 1996;**80**:969–77.
40. Steinsvik S, Bugge R, Gjonnes J, Tafto J, Norby T. The defect structure of $SrTi_{1-x}Fe_xO_{3-y}$ ($x = 0$–0.8) investigated by electrical conductivity measurements and electron energy loss spectroscopy (EELS). *J Phys Chem Solids* 1997;**58**:969–76.
41. Chan N-H, Smyth DM. Defect chemistry of $BaTiO_3$. *J Electrochem Soc* 1976;**123**:1584–5.
42. Chan N-H, Sharma RK, Smyth DM. Nonstoichiometry in un-doped $BaTiO_3$. *J Am Ceram Soc* 1981;**64**:556–62.
43. Ridpath DL, Wright DA. Electrical conductivity of reduced barium titanate crystals. *J Mater Sci* 1970;**5**:487–91.
44. Ihrig H, Hennings D. Electrical transport properties of *n*-type $BaTiO_3$. *Phys Rev B* 1978;**17**:4593–9.
45. Iguchi E, Kubota N, Natamori T, Yamamoto N, Lee KJ. Polaronic conduction in *n*-type $BaTiO_3$ doped with La_2O_3 and Gd_2O_3. *Phys Rev B* 1991;**43**:8646–9.
46. Yoon S, Pithan C, Waser R, Dornseiffer J, Xiong Y, Grüner D, et al. Spark plasma sintering and electronic conduction mechanism in $BaTiO_3$–Ni composite. *J Am Ceram Soc* 2010;**93**:4075–80.